Zebralike Patterned Organic Conductor with Periodic Modulation of Mobility and Peierls Transition

M. Drescher,[1,*] N. Kaplan,[2] and E. Dormann[1]
[1]*Physikalisches Institut, Universität Karlsruhe (TH), D-76128 Karlsruhe, Germany*[†]
[2]*Racah Institute of Physics, Hebrew University, Jerusalem, Israel*
(Received 23 April 2004; published 7 January 2005)

We manipulated the defect concentration in a (fluoranthene)$_2$PF$_6$ crystal by proton irradiation through a periodic grid, resulting in a striped defect pattern. Spatially resolved pulsed *X*-band ESR analysis was used to quantify the resulting *local* defect concentrations, spin diffusion coefficients, and electron spin concentrations. The temperature dependence of the data proves that spin diffusion coefficient and Peierls transition can be tailored in a controlled way via the defect concentrations.

DOI: 10.1103/PhysRevLett.94.016404 PACS numbers: 71.30.+h, 61.80.Jh, 72.15.Lh, 76.30.Pk

Since the early investigations of charge density wave (CDW) fluctuations and the Peierls transition in quasi-one-dimensional (1D) conductors, the influence of defects has been a matter of concern [1–3]. Full quantum mechanical calculations described also the structural changes in finite Peierls systems quantitatively [4]. Organic conductors based on one-dimensionally stacked radical cations of aromatic pure hydrocarbons (arenes) are highly anisotropic conductors, with conductivity anisotropy reaching 10^4:1. Their Peierls transition temperatures, in the range up to 200 K, results from 3D Coulomb interaction of phonon coupled 1D CDW fluctuations, with a prominent role played by the complex anions, like PF_6^- [5]. Radical-cation salts like (fluoranthene)$_2$PF$_6$ [(FA)$_2$PF$_6$] open thus the possibility to modify the conduction electron mobility (or the spin diffusion coefficient D) and the Peierls transition temperature T_P by the introduction of defects via their structural sensitivity to radiation [6,7]: 1% of defects reduces $D_\parallel$ by about a factor of 50 [8], and T_P by about 50 K [9]. Unfortunately, the transport properties of (FA)$_2$PF$_6$ are notoriously sample and ''aging'' dependent. To enable critical investigation of these properties, it is imperative to study the effects of defect concentration all in one and the same crystal simultaneously, for example, by spatially modulating the defect concentration. We describe here the first successful temperature dependent experiment which verifies directly the spatial modulation of $D_\parallel$ and T_P, resulting from radiation modulation, in a single crystal of the organic conductor (FA)$_2$PF$_6$.

The fascinating electron spin dynamics of the quasi-1D organic conductor (FA)$_2$PF$_6$ is dominated by a highly anisotropic diffusion tensor of the conduction electrons, due to the crystal structure [10], as well as by the Peierls transition from the metallic to a semiconducting Peierls phase ($T_P = 186$ K). Pulsed conduction electron spin resonance is possible, because the spin-orbit coupling of the charge carriers is weak and therefore the ESR lines are narrow. ''Pure'' as-grown crystals exhibit regions where free diffusion of the conduction electron spin is possible from one end of the crystal to the other [11]. Paramagnetic defects contribute to the ESR signal and affect drastically the spin dynamic properties.

The electron spin susceptibility and thus T_P and the mobility (diffusion coefficient D) both can be determined by magnetic resonance techniques [12–14]. An especially clear-cut way to demonstrate the ability to tailor mobility and Peierls transition arbitrarily is to prepare a sample with alternating zones of low and high concentrations of defects along the conduction direction of one selected crystal. With such a sample, the variation of the investigated properties should be spatially resolved using 1D magnetic resonance imaging techniques [15,16].

A high-quality crystal (defect concentration $x \approx 0.05\%$) of this radical-cation salt of 1.5 mm length has been irradiated with energetic protons ($E_P = 25$ MeV) via a grid resulting in a striped pattern (Fig. 1). Stripes of a thickness of 100 μm are alternately irradiated or screened from irradiation as described in [17]. To analyze the dynamic properties of the electron spins in this Peierls sys-

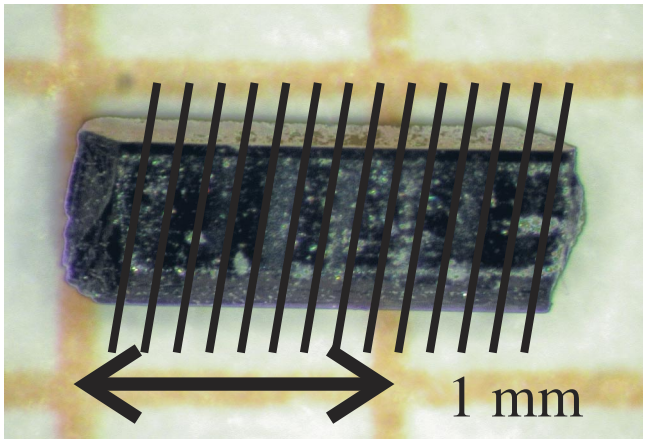

FIG. 1 (color online). Optical photography of the irradiated (FA)$_2$PF$_6$ single crystal. The solid lines are guides to the eye [17].

tem, pulsed X-band ESR measurements were performed. In order to obtain a spatially resolved signal as well as to extract the electron spin diffusion coefficient, a magnetic field gradient ($G = 0.73$ T/m) parallel to the static magnetic field ($B_0 \approx 0.35$ T) was applied. Thus, the local Larmor frequency, dependent on the z position, is given as

$$\omega(z) = \gamma B_0 + \gamma G z. \tag{1}$$

We used a Hahn spin echo ($\frac{\pi}{2} - \tau - \pi$) sequence with a $\frac{\pi}{2}$ pulse length of 12 ns and a detection bandwidth of 200 MHz. According to Eq. (1), and using the concept of reciprocal space vector $\vec{k} = \frac{1}{2\pi}\gamma\vec{G}t$ [15,16], an inverse 1D Fourier transformation of the time-domain echo signal results in a frequency-domain signal; hence a spatial resolution in the z direction is achieved:

$$\mathcal{M}(z, 2\tau) = \int S(k) e^{-i2\pi k z} dk. \tag{2}$$

The echo attenuation in the presence of a magnetic field gradient is affected by relaxation and spin diffusion. The contribution of an individual z slice of Eq. (2) can be parametrized for short τ values by

$$\mathcal{M}_i(2\tau) = \mathcal{M}_i(0)\Big[a \exp\Big(-\frac{2\tau}{T_{2,\mathrm{loc}}}\Big) + (1-a) \times \exp\Big(-\frac{2\tau}{T_{2,\mathrm{del}}} - \frac{2}{3}\gamma^2 G^2 D \tau^3\Big)\Big], \tag{3}$$

assuming there is a fraction "a" of localized spins as well as a fraction "$1 - a$" of delocalized free diffusing electron spins with transverse relaxation times $T_{2,\mathrm{loc}}$ and $T_{2,\mathrm{del}}$, respectively.

Fitting the data in the range $0.2 \le \tau \le 10$ μs with Eq. (3) allows extrapolation of the ESR signal to pulse separation time $\tau = 0$, corresponding with the ESR susceptibility and not affected by relaxation or diffusion phenomena. The extrapolated signal is shown in Fig. 2 for

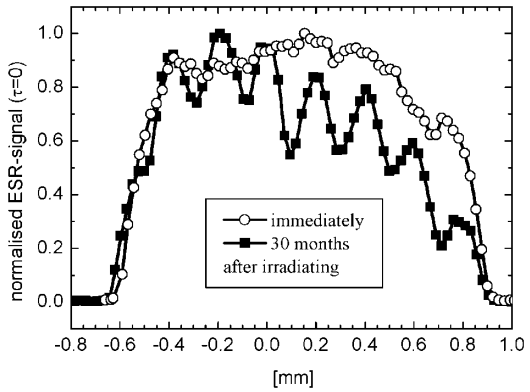

FIG. 2. The ESR susceptibility of irradiated $(FA)_2PF_6$ at $T = 250$ K. The total crystal length of 1.5 mm is represented by 62 slice data points. Only the combined influence of irradiation and aging changed the magnetic moment density. See text for further details.

measurements at $T = 250$ K. The spin density projected onto the z axis reflects the total crystal length of 1.5 mm in 62 data points. Almost no effect on the magnetic moment density was observed immediately after irradiation (circular points). However, some 30 months later we observed the strongly modulated spin density shown by the black squares symbols. The aging effect is caused by increased defect concentration, as we show below. That a crystal of reasonable condition survived after this long time at all demonstrates the excellent crystal quality. The temperature dependence of the susceptibility is caused by the rivalry of two contributing spin systems, namely, the defect spins which follow a Curie-Weiss law and the conduction electrons, with or without Peierls transition. Thus, the ESR susceptibility at any given z position can be expressed as

$$\chi_{\mathrm{ESR}} = \chi_{\mathrm{Curie}} + \chi_{ce}. \tag{4}$$

Allowing for the Peierls transition at T_P, above T_P the Lee-Rice-Anderson (LRA) model characterizes the CDW fluctuations preceding the transition [1], whereas below T_P the conduction electron susceptibility is dominated by an opening energy gap which can be parametrized for $(FA)_2PF_6$ with sufficient accuracy by a model of thermally activated paramagnetism [18]:

$$\chi_{ESR} = \begin{cases} \frac{C}{T-\Theta} + \chi_{\mathrm{LRA}}(T), & T \ge T_P, \\ \frac{C}{T-\Theta} + \chi_{\mathrm{LRA}}(T_P)\frac{T_P}{T}\exp[\frac{\Delta E}{k_B}(\frac{1}{T_P} - \frac{1}{T})], & T \le T_P. \end{cases} \tag{5}$$

The low-temperature expression is written in the form ensuring the continuous variation of $\chi_{\mathrm{ESR}}(T)$ at T_P. The relative temperature dependence of χ_{LRA} was parametrized adapting the mean-field temperature value of $T_{\mathrm{MF}} \approx 400$ K. The effective energy gap describing $\chi_{\mathrm{ESR}}(T)$ for $T < T_P$ was determined to be $\Delta E \approx 1000$ K, but should not be mixed up with the actual low-temperature energy gap. The Curie-Weiss temperature amounts to $\Theta \approx 1.5$ K, which is within the error bar of the temperature T. Quite nicely, the irradiation pattern with its known 100 μm grid can be recognized in the spatially resolved modulated ESR signal. According to Eq. (5), the drastic influence of the temperature effects a complete contrast inversion of the ESR susceptibility as shown in Fig. 3. Fitting the temperature behavior of each data point with Eq. (5) and scaling the amount of the Pauli susceptibility included in the LRA model to the known limiting value of $\chi_{\mathrm{Pauli}} = 132.5 \times 10^{-6}$ $\frac{\mathrm{emu}}{\mathrm{mol}}$ [18] makes it possible to determine the absolute Curie constant

$$C = \frac{N\gamma^2\hbar^2 S(S+1)}{3k_B} \tag{6}$$

and therewith the spatial distribution of the defect concentration of localized electron spins with $S = \frac{1}{2}$ and gyromagnetic ratio γ. While the averaged defect concentration increased by the irradiation immediately from 0.05% to 1%, the 30 months of aging after the irradiating effected

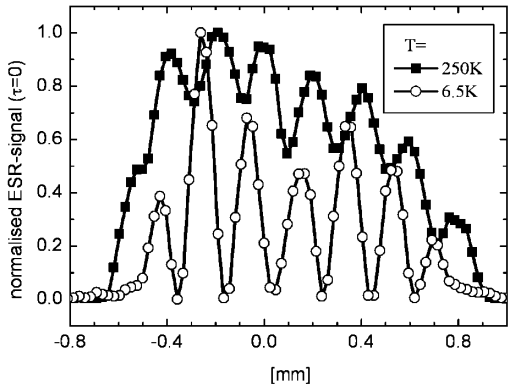

FIG. 3. The ESR signal reflecting the 100 μm grid. Changing the dominating spin system (being either Curie defects or conduction electrons, according to the relevant temperature) causes contrast inversion. Irradiated areas exhibit a strong ESR signal in the low-temperature range.

another increased up to averaged 2%. The spatial distribution of these defects is plotted in Fig. 4, the irradiated areas exhibiting a threefold defect concentration compared to the nonirradiated regions. Figure 4 proves that, indeed, we succeeded in preparing a sample which allows us to study the consequences of varying defect concentration by up to a factor of 3 simultaneously on one individual single crystal. It is important to note that the irradiation induced intrastack localized defects are arene radical cations with even longer spin lattice relaxation time than the delocalized electrons, but with the familiar g tensor of $(FA)_2^{+\bullet}$. Thus, in contrast to most earlier defect studies [2,3], these defects do not increase spin-orbit scattering of the conduction electrons.

Because of the special crystal structure of $(FA)_2PF_6$, the electron spin diffusion exhibits a strong anisotropy of $\frac{D_\parallel}{D_\perp} >$ 3600 [9], a ratio which is reduced by the proton irradiation to below 100 [8]. Figure 5, in combination with Fig. 4, shows the crucial influence of the defects on $D_\parallel$. The increase of defect concentration immediately after irradiating and further during the later aging process constricted the mobility. Even for the 30 month aged crystal the difference between damaged and undamaged regions is about a factor of 4. This loss of diffusivity is caused by the necessity for the spins to change the conducting stack in order to circumvent the defect. The behavior of D as presented here is in full qualitative agreement with expectations based on the result presented in Fig. 4.

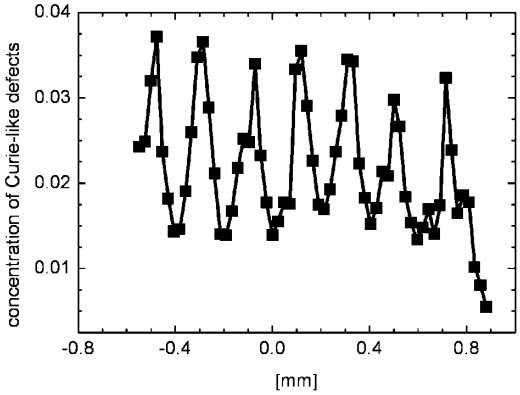

FIG. 4. The irradiated areas exhibit a threefold Curie-defect concentration [calculated from Curie constant and Pauli paramagnetism, Eqs. (5) and (6)].

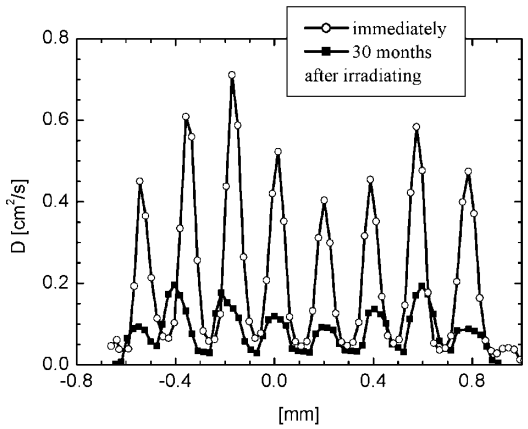

FIG. 5. Electron spin diffusion is effectively reduced by defects. The spatially varying, as well as the time dependent increasing defect concentration, reduces the diffusion coefficient.

The temperature dependence of the normalized ESR susceptibility of individual slices of the crystal is shown in Fig. 6. The Peierls transition can clearly be observed in the curves with circular symbols, representing five different nonirradiated regions. A fit according to Eq. (5) is plotted as a solid, thick line in the same diagram. In contrast, there are five examples of slices from irradiated areas (square black symbols) where a constant ESR susceptibility across T_P of the nonirradiated areas was found.

The results presented in Fig. 6 complete our case. We demonstrated that 1D magnetic resonance imaging can be

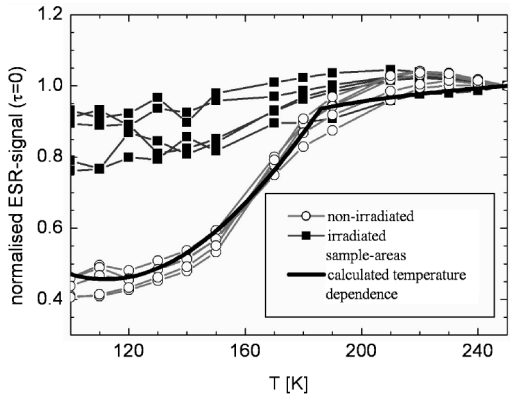

FIG. 6. Comparing the experimental ESR susceptibility between irradiated (five exemplary slices) and nonirradiated (five exemplary slices) areas shows the suppression of the Peierls transition by high defect concentration. The solid line shows a typical result of fitting one particular nonirradiated slice with Eq. (5).

performed for temperatures varying between 250 and 6.5 K. Paramagnetic susceptibility, relaxation times, and the electron spin diffusion coefficient can thus be spatially resolved along the conduction direction in the quasi-one-dimensional organic conductor $(FA)_2PF_6$. By high energy proton irradiation, here for simplicity through an appropriately structured grid, a spatially modulated concentration of paramagnetic defects could be introduced in one and the same crystal, and the influence of long-time aging could be monitored as well. In the metallic phase, the tailored spatial modulation of the mobility (diffusion coefficient $D_{\|}$) of the conduction electrons could be shown. Furthermore, combining the experimental defect concentration data of Fig. 4 with the experimental temperature dependence of the electron spin density shown in Fig. 6, we could verify that the Peierls transition is suppressed in the slices containing a high concentration of defects while remaining around $T_P = 185$ K for nonirradiated regions in the very same crystal. This opens access to arbitrary tailoring and experimental verification of spatially varying conduction electron mobilities and metal-semiconductor transitions in organic conductors.

We thank J. Gmeiner for growing this crystal, and A. Feintuch and T. Wokrina for discussions. This project was financially supported by the DFG (Do 181/10). One of us (N. K.) acknowledges financial support by the Israel Science Foundation (Grant No. 28/01).

*Electronic address: Malte.Drescher@pi.uka.de
†Electronic address: http://www-pi.physik.uni-karlsruhe.de/index_en.html

[1] P. A. Lee, T. M. Rice, and P. W. Anderson, Phys. Rev. Lett. **31**, 462 (1973).
[2] B. R. Patton and L. J. Sham, Phys. Rev. Lett. **33**, 638 (1974).
[3] D. Jerome and H. Schulz, Adv. Phys. **31**, 299 (1982).
[4] I. Baldea, H. Köppel, and L. S. Cederbaum, J. Phys. Soc. Jpn. **68**, 1954 (1999).
[5] C. Buschhaus, R. Moret, S. Ravy, and E. Dormann, Synth. Met. **108**, 21 (2000).
[6] M. Sanquer, S. Bouffard, and L. Forro, Mol. Cryst. Liq. Cryst. **120**, 183 (1985).
[7] N. Mermilliod and N. Sellier, J. Phys. (Paris), Colloq. **44**, C3-1353 (1983).
[8] T. Wokrina, J. Gmeiner, N. Kaplan, and E. Dormann, Eur. Phys. J. B **35**, 191 (2003).
[9] M. Drescher, D. S. de Jauregui, S. Matejcek, and E. Dormann, Proceedings of ICSM 2004 [Synth. Met. (to be published)].
[10] V. Enkelmann, B. S. Morra, C. Kröhnke, G. Wegner, and J. Heinze, J. Chem. Phys. **66**, 303 (1982).
[11] G. Alexandrowicz, T. Tashma, A. Feintuch, A. Grayevsky, E. Dormann, and N. Kaplan, Phys. Rev. Lett. **84**, 2973 (2000).
[12] M. Mehring, *Low Dimensional Conductors and Superconductors* (Plenum Publishing Corp., New York, 1987), edited by D. Jerome and L. G. Caron.
[13] G. G. Maresch, A. Grupp, M. Mehring, J. U. von Schütz, and H. C. Wolf, J. Phys. (Paris) **46**, 461 (1985).
[14] G. G. Maresch, A. Grupp, M. Mehring, and J. U. von Schütz, Synth. Met. **16**, 161 (1986).
[15] P. T. Callaghan, *Principles of Nuclear Magnetic Resonance Microscopy* (Oxford Science Publications, Oxford, 1995).
[16] P. Mansfield and P. K. Grannell, Phys. Rev. B **12**, 3618 (1975).
[17] T. Wokrina, J. Gmeiner, N. Kaplan, and E. Dormann, Phys. Rev. B **67**, 054103 (2003).
[18] U. Köbler, J. Gmeiner, and E. Dormann, J. Magn. Magn. Mater. **69**, 189 (1987).